


# Assessing the physical reality of Milky Way open cluster candidates

Andrés E. Piatti <sup>1,2,3</sup>★ Denis M. F. Illesca,<sup>1,2,3</sup> Agustina A. Massara,<sup>3</sup> Matías Chiarpotti,<sup>3</sup> Daiana Roldán,<sup>3</sup> Micaela Morón<sup>3</sup> and Fabrizio Bazzoni<sup>3</sup>

<sup>1</sup>*Instituto Interdisciplinario de Ciencias Básicas (ICB), CONICET-UNCUYO, Padre J. Contreras 1300, M5502JMA Mendoza, Argentina*

<sup>2</sup>*Consejo Nacional de Investigaciones Científicas y Técnicas, Godoy Cruz 2290, C1425FQB Buenos Aires, Argentina*

<sup>3</sup>*Facultad de Ciencias Exactas y Naturales, Universidad Nacional de Cuyo, Padre J. Contreras 1300, M5502JMA Mendoza, Argentina*

Accepted 2022 November 23. Received 2022 November 15; in original form 2022 September 12

## ABSTRACT

We report results on the analysis of 11 new Milky Way open cluster candidates, recently discovered from the detection of stellar overdensities in the Vector Point diagram, by employing Xtreme deconvolution Gaussian mixture models. We treated these objects as real open clusters and derived their fundamental properties with their associated intrinsic dispersions by exploring the parameter space through the minimization of likelihood functions on the generated synthetic colour–magnitude diagrams. The intrinsic dispersions of the resulting ages turned out to be much larger than those usually obtained for open clusters. Indeed, they resemble the ages and metallicities of composite star field populations. We also traced their stellar number density profiles and mass functions and derived their total masses and Jacobi and tidal radii, which helped us as criteria while assessing their physical nature as real open clusters. Because the 11 candidates show a clear gathering of stars in the proper-motion plane and some hint for similar distances, we concluded that they are possibly sparse groups of stars.

**Key words:** techniques: photometric – open clusters and associations: general.

## 1 INTRODUCTION

Tons of data have been made available from sky surveys that have allowed us to embark in searches for new open cluster candidates (Ivanov et al. 2017; Torrealba, Belokurov & Koposov 2019); among them are *Gaia* (Babusiaux et al. 2022), SMASH (Nidever et al. 2021), VVV (Minniti et al. 2010), etc. The background motivation for such an endeavour comprises, among others, the knowledge of the Milky Way open cluster system (Dias et al. 2021); the recovery of the Milky Way disc star formation history (Anders et al. 2021); the trace of Galactic spiral-arm sub-structures (Cantat-Gaudin et al. 2020), etc. To explore and exploit such a giant data volume, automatic computer-based engines have been developed (Castro-Ginard et al. 2021; Hunt & Reffert 2021). These search engines deal with the recognition of overdensities of stars in an  $N$ -dimensional space, including proper motions, parallaxes, photometric properties, sky positions, etc., as independent dimensions (variables). Their success in identifying new open cluster candidates has varied depending on the engines' complexity.

Recently, Jaehnig, Bird & Holley-Bockelmann (2021) applied Xtreme deconvolution Gaussian mixture models on *Gaia* Data Release 2 proper motions and parallaxes (Gaia Collaboration 2016, 2018) and identified 11 previously uncovered Vector Point diagrams' overdensities, which occupy a compact volume in the proper-motion space. The stars populating these overdensities are distributed in the colour–magnitude diagram (CMD) resembling those of open clusters. Based on this similarity, they performed theoretical isochrone fits and derived representative red-

dening, ages, and distances. Nevertheless, they stressed the status of these 11 objects as open cluster candidates and made clear that detailed analyses are needed in order to confirm them as bona fide open clusters. They called them XDOCCs (Xtreme deconvolution open cluster candidates) and numbered them from #1 to #11.

Looking at their stellar distributions in the Galactic coordinate system (see figs 9–11 in Jaehnig et al. 2021), most of the XDOCCs do not show the expected King's (1962) profile (Piskunov et al. 2007; Kharchenko et al. 2013) but stars scattered across the analyzed field. This appearance led us to remind that field stars may also distribute in the CMD, giving the appearance of the star sequence of an open cluster, as Burki & Maeder (1973) have shown. Therefore, the presence of star sequences in CMDs should not be taken as a direct proof of the existence of a real open cluster. Relatively faint field star main sequences, for example, can mimic the lower part of open cluster main sequences. Precisely, the aim of this work consists of revisiting the 11 XDOCCs and providing with an assessment on their nature as genuine open clusters. The present results highlight the importance of considering not only the proper motions' distribution to conclude on the existence of a physical system but also its spatial distribution, size, mass, etc.

In Section 2, we estimate XDOCC fundamental parameters disentangling observational errors from the intrinsic dispersion and compare the resulting values with those derived by Jaehnig et al. (2021). We also discuss different astrophysical aspects that arise from considering the available data to conclude on the unsupported existence of new open clusters. In Section 3, we summarize the main conclusions of this work and suggest some sanity-check analysis for future searches of open cluster candidates.

\* E-mail: [andres.piatti@unc.edu.ar](mailto:andres.piatti@unc.edu.ar)

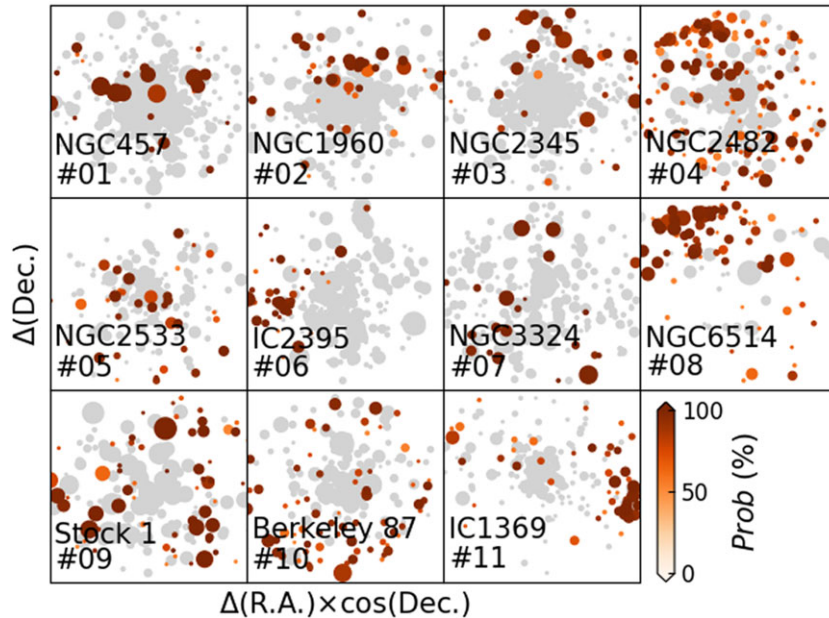


**Figure 1.** Sky charts of stars with assigned membership probability (Prob) higher than 50 per cent projected on the field of known open clusters (grey symbols) and XDOCCs (coloured symbols), respectively. The size of the symbols is proportional to the star brightness. Each panel, centred on the known open cluster, indicates its name and the number of the XDOCC.

**Table 1.** Assessments on the reality of XDOCCs as open clusters.

Name	Sky chart	Size and mass	Radial profile	CMD	Adopted
XDOCC-01	N	Y	N	N	N
XDOCC-02	N	N	N	N	N
XDOCC-03	N	N	N	N	N
XDOCC-04	N	N	N	N	N
XDOCC-05	N	Y	N	N	N
XDOCC-06	Y	N	N	N	N
XDOCC-07	N	Y	N	N	N
XDOCC-08	Y	N	N	N	N
XDOCC-09	N	N	N	N	N
XDOCC-10	N	N	N	N	N
XDOCC-11	Y	N	N	N	N

## 2 DATA ANALYSIS AND DISCUSSION

For comparison purposes with the work by Jaehnig et al. (2021), we employed their same data sets, which include stars with assigned membership probabilities higher than 50 per cent. Since the 11 XDOCCs that were identified projected on the field of 11 known open clusters, we also retrieved the same information for them. We started by constructing schematic sky charts for the 11 XDOCCs, which we depict in Fig. 1. Stars of the known open clusters were drawn with light-grey filled circles and those of the 11 XDOCCs with coloured ones, according to their membership probability. We represented the stars with circles of different sizes, which are proportional to the star brightness. Each panel is centred on the known open cluster, and its size is such that it includes all the retrieved stars in the field. At first glance, the known open clusters are clearly visible, with the sole exception of NGC 6514 (middle-right panel), which is a diffuse nebula known as the ‘Trifid’ Nebula (Glushkov & Karyagina 1984). As for the 11 XDOCCs, their appearances do not seem to resemble those of real open clusters, with some exceptions. Indeed, although open clusters can have stars spatially sparsely distributed in comparison with those in globular clusters, they all have a core

(central) region of higher stellar density. Open clusters also usually show brighter stars more centrally concentrated than fainter stars. Based on these qualitative descriptions of an open cluster, we distinguished those XDOCCs with a chance of being real stellar aggregates from those that seem more probably to be the result of a superposition of stars aligned along the line of sight. We included such a classification in Table 1 with a Y or N, respectively.

### 2.1 Stellar mass functions

Joshi et al. (2016) derived a relationship between open cluster mass and size that we used to probe the reality of the 11 XDOCCs as physical systems. By assuming that they are open clusters, we first constructed their mass functions from which we estimated an upper limit for their initial total masses. In order to do that, we used stars with membership probabilities higher than 50 per cent and 90 per cent, respectively, with the aim of evaluating mass-function uncertainties. While counting the number of stars per mass interval, we adopted a mass bin of  $\log(M/M_{\odot}) = 0.05$ . The individual stellar masses were interpolated using the theoretical isochrones computed

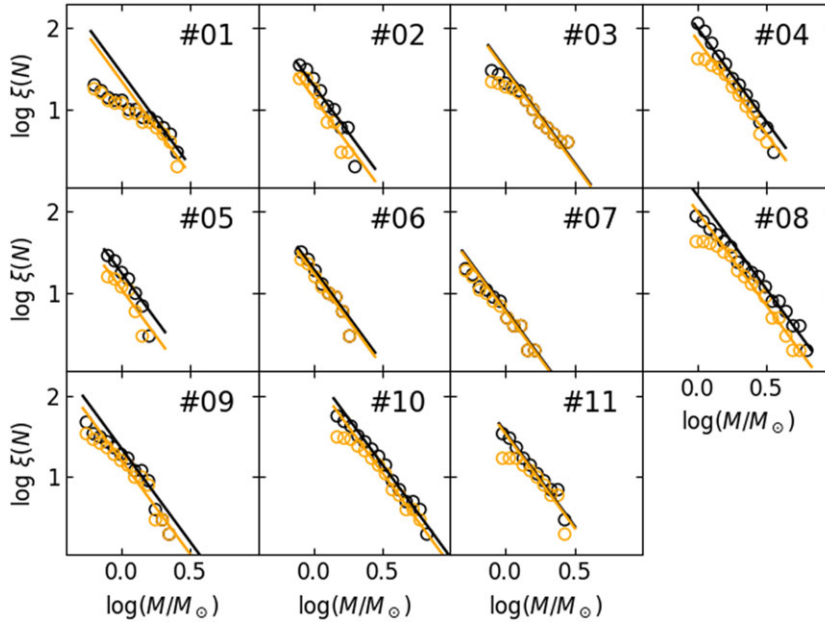


**Figure 2.** Mass function of the XDOCCs, with the corresponding numbers labelled in the respective panels. Black and orange circles correspond to mass functions built from stars with membership probabilities higher than 50 per cent and 90 per cent, respectively. The coloured straight lines match the respective mass distributions.

by Bressan et al. (2012, PARSEC v1.2S<sup>1</sup>), the *Gaia* *G* magnitudes, and the ages, distances, and interstellar absorptions  $A_V$  derived for the 11 XDOCCs by Jaehnig et al. (2021). The resulting mass functions are shown in Fig. 2, where we distinguished with black and orange open clusters those built for stars with membership probabilities higher than 50 per cent and 90 per cent, respectively. As can be seen, there are only small differences between them. We then matched on them a Kroupa’s (2002) mass-function profile, which in turn we used to compute the total mass for stars more massive than  $0.5 M_\odot$ . We then computed the XDOCCs’ Jacobi radii using the expression (Spitzer 1987)

$$R_J = \left( \frac{M_{\text{XDOCC}}}{3M_{\text{MW}}} \right)^{1/3} \times R_{\text{GC}}, \quad (1)$$

where  $M_{\text{XDOCC}}$  is the XDOCC’s mass derived above, and  $M_{\text{MW}}$  is the Milky Way mass comprised within a radius equal to the XDOCC’s Galactocentric distance ( $R_{\text{GC}}$ ). The  $R_{\text{GC}}$  values were taken from Jaehnig et al. (2021), while  $M_{\text{MW}}$  values were interpolated in the Milky Way mass versus Galactocentric relationship obtained by Bird et al. (2022). We obtained two different  $R_J$  values using the derived XDOCC’s mass estimates for membership probabilities higher than 50 per cent and 90 per cent, respectively. We included these values as labels in the different panels of Fig. 3.

The resulting  $M_{\text{XDOCC}}$  and  $R_J$  ranges were plotted in Fig. 4 as horizontal and vertical segments, respectively, where we also included the radius versus mass relationship obtained by Joshi et al. (2016). We used the loci of the XDOCCs in Fig. 4 as an additional criterion for assessing on their physical reality as open clusters. Particularly, objects that fall within a  $3\sigma$  confidence interval (XDOCC 01, 05, and 07) were considered as possible real systems, and for them, we included a Y in Table 1.

<sup>1</sup><http://stev.oapd.inaf.it/cgi-bin/cmd>

## 2.2 Stellar number density profiles

In order to quantify the visual appearance of the 11 XDOCCs (see Fig. 1), we built their stellar number density profiles. To do this, we counted the number of stars in the annuli centred on the XDOCCs of width 0.050, 0.067, 0.100, and 0.200 times their Jacobi radii (for membership probabilities higher than 90 per cent), respectively, and then averaged all the obtained density values, previously rebinned from interpolation, and computed their standard errors. The resulting binned number density profiles are shown in Fig. 3, where we used the ratio between the distance to the XDOCC’s centre and the Jacobi radius for comparison purposes. In addition, dealing with  $R_J$  values allows us to evaluate the level of star-mass segregation and to probe whether there are unbound stars among those identified as XDOCC members (Küpper et al. 2010). The latter is an interesting aspect to analyse, given the sparse appearance of the 11 XDOCCs.

The stellar radial profile of an open cluster is expected to follow a King’s (King 1962) model (Piskunov et al. 2007; Kharchenko et al. 2013, and references therein), as follows:

$$f(r) = k \times \left( \frac{1}{\sqrt{1 + (r/r_c)^2}} - \frac{1}{\sqrt{1 + (r_t/r_c)^2}} \right)^2, \quad (2)$$

where  $k$  is a constant and  $r_c$  and  $r_t$  are the core and tidal radii, respectively. Equation (2) implies that there are not any clusters’ members beyond  $r_t$ . Likewise,  $r_t$  cannot be larger than the derived  $R_J$ . Recently, Zhong et al. (2022) have showed that a two-component model with a King’s core distribution and a logarithmic Gaussian outer halo distribution describe better the internal and external structural features of open clusters. They found that core, half-mass, tidal and Jacobi radii are statistically linearly related, which suggests that the inner and outer regions of the clusters are interrelated and follow similar evolutionary processes. Because none of the XDOCCs’ number density profiles of Fig. 3 resembles a King’s (King 1962) profile, we concluded that the XDOCCs are not real open clusters and included an  $N$  in the fourth column of Table 1.

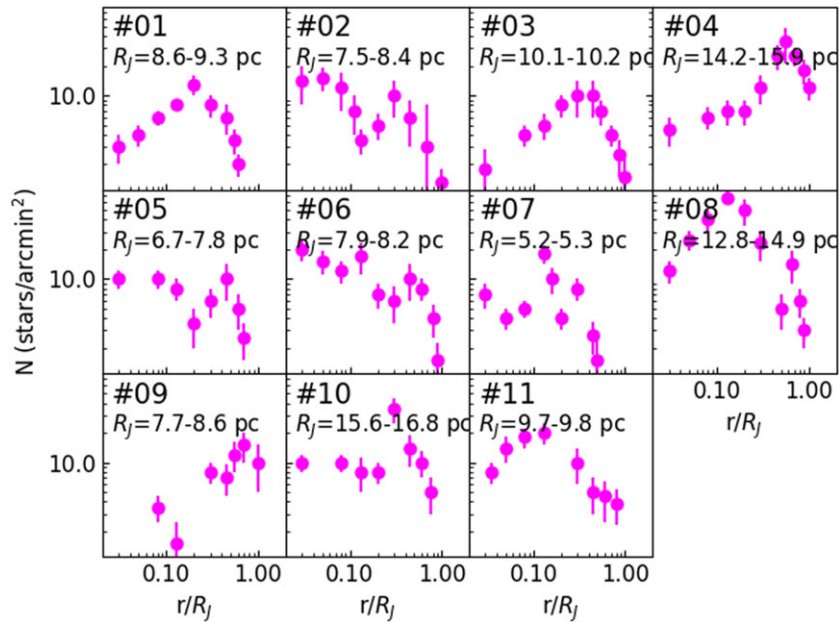


**Figure 3.** Stellar number density profiles of the XDOCCs, with the corresponding numbers labelled in the respective panels. The derived Jacobi radius ranges are also indicated (see the text for details).

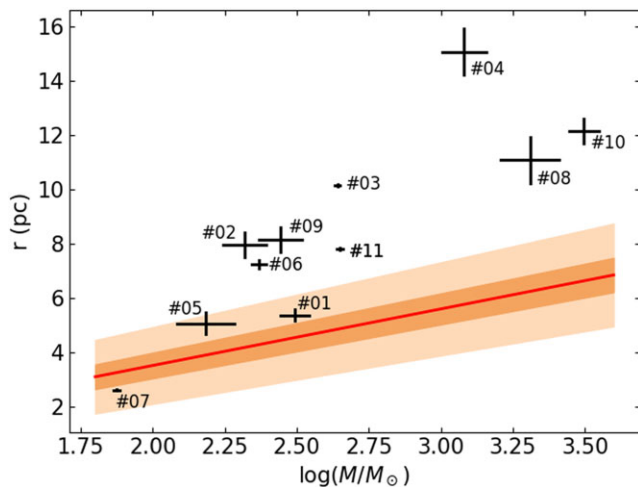


**Figure 4.** Relationship between radii and masses of the 11 XDOCCs. The red line and orange and light-red shaded regions around it represent the relationship derived by Joshi et al. (2016) and the  $1\sigma$  and  $3\sigma$  confidence intervals, respectively. The numbers of the respective XDOCCs are also indicated.

Note that the remarkable drop of the stellar number density profiles towards the inner regions is not caused by crowding effects, because XDOCCs are composed by a relatively sparse group of stars.

### 2.3 Colour–magnitude diagrams

We first obtained individual stellar reddenings through the GALExtin<sup>2</sup> interface (Amôres et al. 2021), by using the Milky Way reddening map of Chen et al. (2019), which was built specifically for *Gaia* bandpasses. We then corrected the *G* magnitudes and  $BP - RP$

colours using the retrieved total absorptions ( $A_G$ ) and the total to selective absorption ratios given by Chen et al. (2019). The absorption uncertainties  $\sigma(A_G)$  span from 0.003 up to 0.020 mag, with an average of 0.010 mag at any  $A_G$  interval. Fig. 5 illustrates the spatial reddening variations for the XDOCC stars, with stars coloured according to their  $E(B - V)$  values, while Fig. 6 depicts the reddening-corrected CMDs.

We performed isochrone fits to the reddening-corrected XDOCCs' CMDs, not assuming a solar metallicity (Jaehnig et al. 2021) but including the metallicity ( $[M/H]$ ), the age, the total mass, and the binary fraction as free parameters. The fundamental parameters were derived by employing specific routines of the Automated Stellar Cluster Analysis code (ASTECA; Perren, Vázquez & Piatti 2015), which is able to derive them simultaneously. ASTECA relies on the construction of a large number of synthetic CMDs from which it finds the one that best resembles the observed CMD. Thus, the metallicity, the age, the distance, the reddening, the star-cluster present mass, and the binary fraction associated to that best representative-generated synthetic CMD are adopted as the best-fitting star-cluster properties.

ASTECA is able to handle a wide range of values of the aforementioned parameters. However, since the stars used share similar parallaxes (see table 1 and figs 9–11 in Jaehnig et al. 2021), we constrained the generation of synthetic CMDs to those with distance moduli around the mean observed parallaxes. We fitted theoretical isochrones computed by Bressan et al. (2012, PARSEC<sup>3</sup>) for the *Gaia* DR2 photometric system. Particularly, we chose PARSEC v1.2S isochrones spanning metallicities ( $Z = 0.0152 \times 10^{[Fe/H]}$ ) from 0.003 up to 0.038 dex, in steps of 0.001 dex and  $\log(\text{age}/\text{year})$  from 7.0 up to 9.0 in steps of 0.025. Because photometric errors are not included in table 2 of Jaehnig et al. (2021), we interpolated them from figs 9–11 in Evans et al. (2018). To derive the errors in the *Gaia* colour, we added in quadrature those of the individually involved magnitudes. We note that reliable photometric uncertainties are needed to uncover the intrinsic dispersion in the CMD. If points in the CMD are used

<sup>2</sup><http://www.galexin.org/>

<sup>3</sup><http://stev.oapd.inaf.it/cgi-bin/cmd>

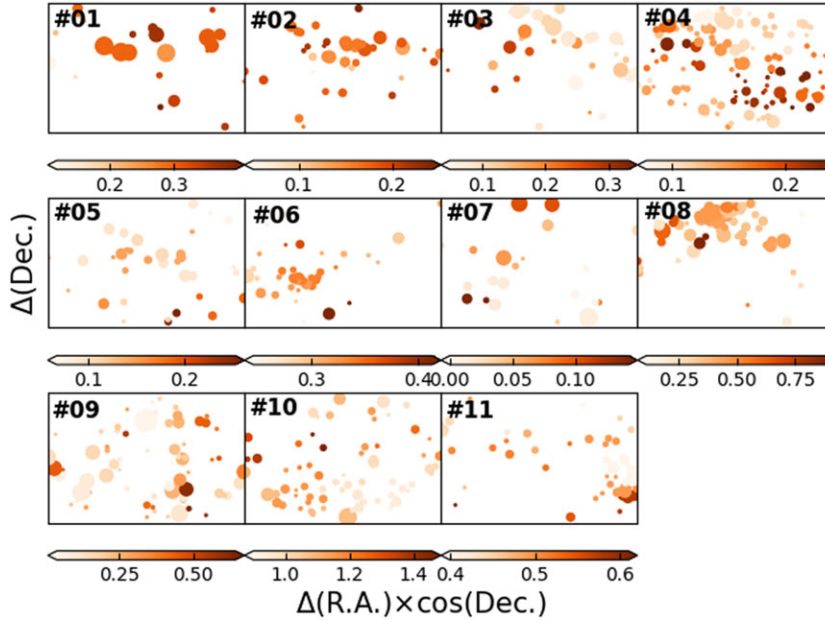


**Figure 5.** Sky charts of XDOCC stars (see Fig. 1); the size of the symbols is proportional to the star brightness. Stars are coloured according to its  $E(B - V)$  value (mag), as shown in the respective colour bar.

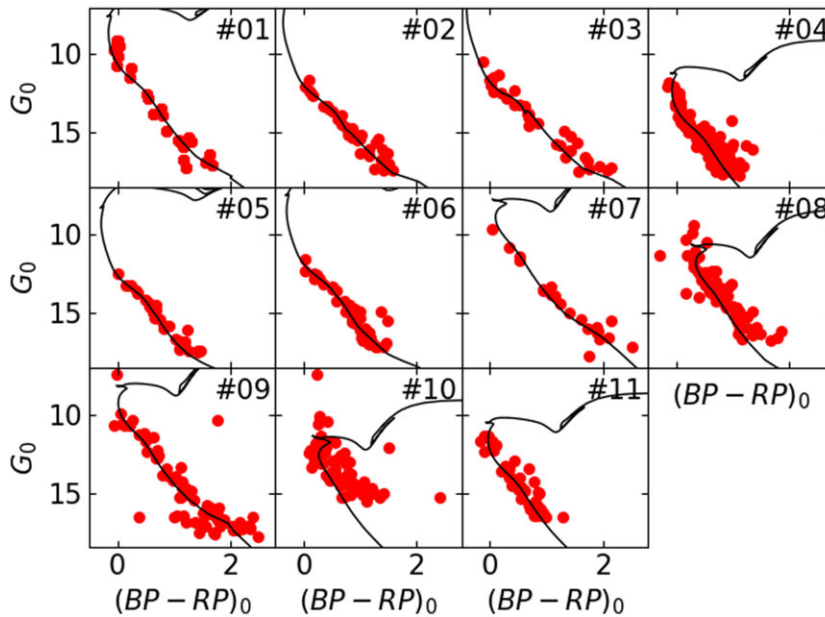


**Figure 6.** Reddening-corrected *Gaia* CMDs of the 11 XDOCCs as labelled in the upper-right corner of the panels. The theoretical isochrone of Bressan et al. (2012, PARSEC v1.2S) corresponding to the parameters given in Table 2 and for the mean observed parallaxes derived by Jaehnig et al. (2021) are superimposed.

without errors, then the observed scatter is considered as the result of the combined intrinsic dispersions of the fundamental parameters (reddening, distance, age, etc). When photometry errors are taken into account, then the resulting astrophysical properties' uncertainties are better constrained. In practice, the intrinsic dispersion should be smaller than the observed photometric ones.

ASTECA generates synthetic CMDs by adopting the initial mass function given by Kroupa (2002) and a minimum mass ratio for the generation of binaries of 0.5. The total observed star-cluster mass and its binary fraction were set in the ranges 100–5000  $M_{\odot}$  and 0.0–0.5, respectively. In brief, ASTECA explores the parameter space of the synthetic CMDs through the minimization of the likelihood function

defined by Tremmel et al. (2013, the Poisson's likelihood ratio, equation 10) using a parallel tempering Bayesian MCMC algorithm and the optimal binning Knuth's (2018) method. The uncertainties associated with the derived parameters are estimated from the standard bootstrap method described in Efron (1982). We refer the reader to Perren et al. (2015), where details related to the implementation of these algorithms are provided. The resulting fundamental parameters are listed in Table 2, and the object CMDs with the isochrone corresponding to those parameter values are illustrated in Fig. 6.

Fig. 6 shows relatively populated to very populous main sequences that extend from  $\sim 4$  up to  $\sim 8$  mag long. They do not show any clear sign of evolution, with the exception of the presence of few stars at the

**Table 2.** ASTECA results for XDOCC objects.

Name	$\text{Log}(t\text{yr}^{-1})$	[Fe/H] (dex)	Mass ( $M_{\odot}$ )	Binary fraction
XDOCC-01	$8.13 \pm 0.28$	$0.40 \pm 0.20$	$213 \pm 89$	$0.38 \pm 0.14$
XDOCC-02	$7.47 \pm 0.43$	$0.24 \pm 0.18$	$343 \pm 122$	$0.45 \pm 0.12$
XDOCC-03	$7.23 \pm 0.48$	$0.25 \pm 0.24$	$189 \pm 93$	$0.17 \pm 0.13$
XDOCC-04	$8.47 \pm 0.06$	$0.23 \pm 0.12$	$1543 \pm 328$	$0.32 \pm 0.10$
XDOCC-05	$7.73 \pm 0.45$	$0.17 \pm 0.19$	$188 \pm 126$	$0.22 \pm 0.15$
XDOCC-06	$7.67 \pm 0.40$	$0.39 \pm 0.15$	$229 \pm 123$	$0.41 \pm 0.12$
XDOCC-07	$8.76 \pm 0.31$	$0.24 \pm 0.24$	$125 \pm 38$	$0.43 \pm 0.13$
XDOCC-08	$8.75 \pm 0.12$	$0.34 \pm 0.12$	$661 \pm 304$	$0.40 \pm 0.12$
XDOCC-09	$8.71 \pm 0.26$	$0.07 \pm 0.19$	$204 \pm 82$	$0.35 \pm 0.13$
XDOCC-10	$8.85 \pm 0.08$	$0.40 \pm 0.17$	$655 \pm 288$	$0.29 \pm 0.12$
XDOCC-11	$8.48 \pm 0.37$	$0.37 \pm 0.15$	$591 \pm 165$	$0.29 \pm 0.14$

main sequence turn-off of XDOCC-08. Although the best representative isochrones satisfactorily reproduce these long main sequences, there is no star in more evolved stellar evolutionary phases, as we expect in open clusters with populous main sequences. Indeed, by using the Padova group web interface,<sup>4</sup> we generated synthetic CMDs of open clusters having the total masses, ages, and metallicities derived for the 11 XDOCCs and found that they show 1–2 red clump stars and very well populated main sequence turn-off regions.

As Burki & Maeder (1973) have shown, a composite star field population can mimic in the CMD the appearance of an open cluster’s star sequence. Disentangling whether this is the case of the XDOCCs’ CMDs (Fig. 6) is difficult to accomplish only from the analysis of those CMDs. However, because of the minimization of likelihood functions used to derive the astrophysical parameters, the derived bootstrapped uncertainties tell us about the level of uniqueness of the representative solutions. Thus, under the presence of relatively tight main sequences and small photometric errors, relatively large parameter uncertainties could suggest that different collections of isochrones are needed to map different parts of the observed main sequence. When dealing with true open clusters, typical intrinsic dispersions of fundamental parameters as estimated by ASTECA (Perren et al. 2022, and references therein) are  $\sigma \log(t/\text{yr}) \approx 0.12$  and  $\sigma[\text{Fe}/\text{H}] \approx 0.21$  dex. Table 2 shows that age uncertainties are notably large in most of the cases, suggesting that a range of ages represents the fitted main sequences. The resulting metallicities are also notably larger than the values of open clusters that follow the metallicity gradient of the Milky Way disc. We used the Galactocentric distances of XDOCCs computed by Jaehnig et al. (2021), the recent age–metallicity–Galactocentric position relationship derived by Magrini et al. (2022) from the *Gaia*-ESO survey (Gilmore et al. 2012), and ages and metallicities of Table 2 to confirm that all XDOCCs fall outside the relationship for open clusters. Finally, the resulting binary fractions (see Table 2) generated by ASTECA are relatively high. This happens when the wider broadness of the main sequence of a composite star field population is assumed to be the main sequence of a star cluster.

## 2.4 Spectroscopic data

Chemical abundances and radial velocities for individual stars are also helpful in order to disentangle whether they belong to the field population or to a stellar aggregate. We took advantage of the Sloan Digital Sky Survey (SDSS) IV DR17, particularly the APOGEE-2

data base (Blanton et al. 2017; Ahumada et al. 2020), to retrieve this information. The spectral parameters provided in the APOGEE-2 database were obtained using the APOGEE Stellar Parameters and Chemical Abundance Pipeline (García Pérez et al. 2016) and were accessed employing the following Structured Query Language query to the SDSS data base server<sup>5</sup>:

```
SELECT TOP 100
  s.apogee_id, s.ra, s.dec, s.glon, s.glat, s.snr,
  s.vhelio_avg, s.verr, a.teff, a.teff_err, a.logg,
  a.logg_err, a.m.h, a.m.h_err, a.alpha.m,
  a.alpha.m_err
FROM apogeeStar as s
JOIN aspcapStar a on s.apstar_id
= a.apstar_id
JOIN dbo.fGetNearbyApogeeStarEq (RA, DEC, 20)
as
  near on a.apstar_id = near.apstar_id
WHERE (a.aspcapflag & dbo.fApogeeAspcapFlag
('STAR_BAD')) = 0
```

We then cross-matched the retrieved APOGEE-2 data sets for the 11 XDOCCs with the corresponding *Gaia* data sets using RA and Dec. coordinates as matching variables and Astropy Project tools.<sup>6</sup> We found only one star in common for XDOCC 10 [2057948152709390848 (*Gaia* DR2 name) == 2M20223036+3712003 (APOGEE-2 name)] with  $T_{\text{eff}} = (16187.49 \pm 647.53)$  K,  $\log(g) = 4.252 \pm 0.082$ , and radial velocity =  $(-18.41 \pm 2.43)$  km s<sup>-1</sup>. No metallicity information is available. By using the derived age, distance, and interstellar absorption of XDOCC 10 (Jaehnig et al. 2021), we found by interpolation into the corresponding theoretical isochrone that the *Gaia* DR2 magnitude and colour resulted to be  $G = 14.16 \pm 0.30$  mag and  $\text{BP} - \text{RP} = 1.38 \pm 0.15$  mag, respectively. These values differ significantly from the observed ones, namely,  $G = 14.654$  mag and  $\text{BP} - \text{RP} = 2.048$  mag. Therefore, we concluded that the star is not at the mean distance of XDOCC 10, although its position in the CMD suggests otherwise. This result points to the need of further spectroscopic data to assess on the physical nature of the 11 XDOCCs. We also note that the individual *Gaia* DR2 parallax uncertainties of the stars selected as members of these objects are still large as to secure a reliable analysis of their distances and hence a 3D structural study of them. With accurate parallaxes, the 3D XDOCCs’

<sup>4</sup><http://stev.oapd.inaf.it/cgi-bin/cmd>

<sup>5</sup><http://skyserver.sdss.org/dr17/SearchTools/sql>

<sup>6</sup><http://www.astropy.org>

dimensions could be estimated, and from them, a comparison with the known size range of real open clusters could be carried out.

### 3 CONCLUDING REMARKS

The number of open cluster candidates identified since recent time from the availability of public databases and computer-based searching techniques is steadily increasing. Likewise, these data sets and analysis methods have been helpful to improve the accuracy of open clusters' fundamental parameters that are re-determined from a homogeneous basis. The outcomes of this promising effort certainly help us to improve our knowledge of the Milky Way open cluster system and hence to better understand the formation and evolution of the disc of our Galaxy.

Recently, Jaehnig et al. (2021) used *Gaia* DR2 data sets to determine the astrophysical properties of 420 known open clusters, by employing Xtreme deconvolution Gaussian mixture models. They also pointed out that other previously unknown 11 open cluster candidates could be populating the searched sky regions. The identification of these new candidates mainly relies on stellar overdensities detected in the Vector Point diagram, whose stars are distributed in CMDs following the appearance of those typical of open clusters; the distribution of parallaxes also turned out to be at first glance compatible with stars being at a similar mean distance. Nevertheless, Jaehnig et al. (2021) stressed that further investigations are necessary in order to confirm their physical nature.

By using the same data sets, we carried out a thorough analysis of these new open cluster candidates (XDOCCs), from which we identified a number of astrophysical aspects that do not fully agree with our present knowledge of the open cluster population. These considerations come from our independent estimates of age, reddening, metallicity, total mass, and binary fraction of the 11 XDOCCs, considering them as real physical stellar systems. These fundamental parameters were derived by disentangling their intrinsic dispersions from the photometric data sets' uncertainties. We obtained astrophysical properties whose associated dispersions are much larger than those usually obtained for open clusters using the same procedure. Such large dispersions are typical of fundamental parameters of composite star field populations.

The apparent distribution of stars in the sky, their projected stellar number density profiles, and the relationship between their masses and projected radii support also, considered all together, the conclusion that the XDOCCs unlikely are real physical systems. We think that this finding highlights the need of gathering more than one criterion when searching for open cluster candidates. Here, we show that a stellar overdensity in the proper-motion space is not enough to conclude on the existence of a stellar aggregate. By relying on a multidimensional approach (3D positions, 3D motions, metallicity, CMD features, etc.), more confidence open cluster candidates will be uncovered. Nevertheless, because of the clearly observed gathering of stars in the Vector Point diagram and some hint for similar distances within the *Gaia* DR2 parallax uncertainties, the XDOCCs could be considered like sparse groups of stars.

### ACKNOWLEDGEMENTS

We thank the referee for the thorough reading of the manuscript and timely suggestions to improve it.

This work has made use of data from the European Space Agency (ESA) mission *Gaia* (<https://www.cosmos.esa.int/gaia>), processed by the *Gaia* Data Processing and Analysis Consortium (DPAC, <https://www.cosmos.esa.int/web/gaia/dpac/consortium>). Funding for the

DPAC has been provided by national institutions, in particular the institutions participating in the *Gaia* Multilateral Agreement.

This work made use of ASTROPY: a community-developed core PYTHON package and an ecosystem of tools and resources for astronomy (Astropy Collaboration 2013, 2018, 2022).

### DATA AVAILABILITY

Data used in this work are available upon request to the author.

### REFERENCES

- Ahumada R. et al., 2020, *ApJS*, 249, 3  
 Amôres E. B. et al., 2021, *MNRAS*, 508, 1788  
 Anders F., Cantat-Gaudin T., Quadrino-Lodoso I., Gieles M., Jordi C., Castro-Ginard A., Balaguer-Núñez L., 2021, *A&A*, 645, L2  
 Astropy Collaboration, 2013, *A&A*, 558, A33  
 Astropy Collaboration, 2018, *AJ*, 156, 123  
 Astropy Collaboration, 2022, *ApJ*, 935, 167  
 Babusiaux C. et al., 2022, preprint ([arXiv:2206.05989](https://arxiv.org/abs/2206.05989))  
 Bird S. A. et al., 2022, *MNRAS*, 516, 731  
 Blanton M. R. et al., 2017, *AJ*, 154, 28  
 Bressan A., Marigo P., Girardi L., Salasnich B., Dal Cero C., Rubele S., Nanni A., 2012, *MNRAS*, 427, 127  
 Burki G., Maeder A., 1973, *A&A*, 25, 71  
 Cantat-Gaudin T. et al., 2020, *A&A*, 640, A1  
 Castro-Ginard A. et al., 2021, *A&A*, 661, A118  
 Chen B. Q. et al., 2019, *MNRAS*, 483, 4277  
 Dias W. S., Monteiro H., Moitinho A., Lépine J. R. D., Carraro G., Paunzen E., Alessi B., Vilella L., 2021, *MNRAS*, 504, 356  
 Efron B., 1982, *The Jackknife, the Bootstrap and Other Resampling Plans*, Society for Industrial and Applied Mathematics, Philadelphia  
 Evans D. W. et al., 2018, *A&A*, 616, A4  
 Gaia Collaboration, 2016, *A&A*, 595, A1  
 Gaia Collaboration, 2018, *A&A*, 616, A1  
 García Pérez A. E. et al., 2016, *AJ*, 151, 144  
 Gilmore G. et al., 2012, *The Messenger*, 147, 25  
 Glushkov Y. I., Karyagina Z. V., 1984, *Tr. Astrofiz. Inst. Alma-Ata*, 44, 43  
 Hunt E. L., Reffert S., 2021, *A&A*, 646, A104  
 Ivanov V. D., Piatti A. E., Beamín J. -C., Minniti D., Borissova J., Kurtev R., Hempel M., Saito R. K., 2017, *A&A*, 600, A112  
 Jaehnig K., Bird J., Holley-Bockelmann K., 2021, *ApJ*, 923, 129  
 Joshi Y. C., Dambis A. K., Pandey A. K., Joshi S., 2016, *A&A*, 593, A116  
 Kharchenko N. V., Piskunov A. E., Schilbach E., Röser S., Scholz R. D., 2013, *A&A*, 558, A53  
 King I., 1962, *AJ*, 67, 471  
 Knuth K. H., 2018, *Astrophysics Source Code Library*, record ascl:803.013  
 Kroupa P., 2002, *Science*, 295, 82  
 Küpper A. H. W., Kroupa P., Baumgardt H., Heggie D. C., 2010, *MNRAS*, 407, 2241  
 Magrini L. et al., 2022, preprint ([arXiv:2210.15525](https://arxiv.org/abs/2210.15525))  
 Minniti D. et al., 2010, *New Astron.*, 15, 433  
 Nidever D. L. et al., 2021, *AJ*, 161, 74  
 Perren G. I., Vázquez R. A., Piatti A. E., 2015, *A&A*, 576, A6  
 Perren G. I., Pera M. S., Navone H. D., Vázquez R. A., 2022, *A&A*, 663, A131  
 Piskunov A. E., Schilbach E., Kharchenko N. V., Röser S., Scholz R. D., 2007, *A&A*, 468, 151  
 Spitzer L., 1987, *Dynamical Evolution of Globular Clusters*, Princeton Univ. Press, Princeton, NJ  
 Torrealba G., Belokurov V., Koposov S. E., 2019, *MNRAS*, 484, 2181  
 Tremmel M. et al., 2013, *ApJ*, 766, 19  
 Zhong J., Chen L., Jiang Y., Qin S., Hou J., 2022, *AJ*, 164, 54

This paper has been typeset from a  $\text{\LaTeX}$  file prepared by the author.